Second Virial Coefficient of Oligo- and Poly(α-methylstyrene)s. Effects of Chain Stiffness, Chain Ends, and Three-Segment Interactions

Wataru Tokuhara, Masashi Osa, Takenao Yoshizaki, and Hiromi Yamakawa*

Department of Polymer Chemistry, Kyoto University, Kyoto 606-8501, Japan

Received April 15, 2003; Revised Manuscript Received May 7, 2003

ABSTRACT: The second virial coefficient A_2 was determined from light scattering measurements for atactic oligo- and poly(α-methylstyrene)s (a-PαMS) with the fraction of racemic diads $f_r = 0.72$ over a wide range of weight-average molecular weight M_w from 6.48×10^2 to 5.46×10^6 in cyclohexane at 30.5 °C (Θ) and in toluene at 25.0 °C, and for $M_w \geq 2 \times 10^5$ in 4-*tert*-butyltoluene at 25.0 °C, in *n*-butyl chloride at 25.0 °C, and in cyclohexane at 35.0, 45.0, and 55.0 °C. It is shown that the observed characteristic features of A_2 at Θ, which is denoted by $A_{2,\Theta}$, as a function of M_w in cyclohexane at Θ, i.e., a sharp increase with decreasing M_w for small M_w and a rather long-tailed negative region for large M_w, may be well explained by the theory that takes account of the effects of chain ends and also of three-segment interactions. It is also shown that the observed dependence of A_2 on M_w in toluene may be quantitatively explained by the theory that takes account of the effects of chain stiffness, local chain conformation, and chain ends. The results for the interpenetration function Ψ appearing in A_2 (without the effects of chain ends) reconfirm that neither the two-parameter (TP) nor the quasi-TP theory can explain the behavior of Ψ, as previously found for atactic polystyrene (a-PS) ($f_r = 0.59$), atactic poly(methyl methacrylate) (a-PMMA) ($f_r = 0.79$), and isotactic PMMA ($f_r \simeq 0.01$); Ψ as a function of the gyration-radius expansion factor depends separately on M_w and the reduced excluded-volume strength. A comparison is made of the present results for $A_{2,\Theta}$ and Ψ in toluene with previous ones for a-PS and a-PMMA in Θ and good solvents.

Introduction

In a series of experimental studies[1] of dilute solution properties of atactic oligo- and poly(α-methylstyrene)s (a-PαMS) with the fraction of racemic diads $f_r = 0.72$, we have recently reported results for the gyration-radius expansion factor[2] α_S and the viscosity- and hydrodynamic-radius expansion factors[3] α_η and α_H, which are concerned with the intramolecular excluded-volume effect. It has been there shown that the behavior of these factors may be well explained in the quasi-two-parameter (QTP) scheme[4] that all the expansion factors are functions only of the intramolecular scaled excluded-volume parameter[4] $\tilde{z}$ instead of the conventional excluded-volume parameter z in the two-parameter (TP) theory.[5] In this paper, we proceed to investigate the behavior of the second virial coefficient A_2, which is concerned with the intermolecular excluded-volume effect, giving major attention to possible effects of chain stiffness and chain ends on it.

The theory[4,6] of A_2 based on the helical wormlike (HW) chain model[4] predicts that neither the TP nor the QTP scheme is valid for the interpenetration function Ψ appearing in A_2 because of chain stiffness, and also that the dependence of A_2 on molecular weight M is remarkably affected, especially for small M, by a chemical difference of the chain ends. The validity of these predictions has already been confirmed in previous experimental papers on A_2 of atactic polystyrene (a-PS),[4,7,8] atactic poly(methyl methacrylate) (a-PMMA),[4,9] and isotactic (i-) PMMA,[10] where the difference in the behavior of Ψ between these polymers has also been semiquantitatively explained by the theory with the values of the HW model parameters[4] determined from an analysis of the unperturbed mean-square radius of gyration $\langle S^2 \rangle_0$ and α_S. The main purpose of the present paper is to examine whether this is also the case with a-PαMS.

In the above-mentioned investigations made so far of A_2 at the Θ temperature, which we denote by $A_{2,\Theta}$, its value $A_{2,\Theta}^{(HW)}$ without the effects of chain ends has been simply set equal to zero in the binary cluster approximation.[5] As pointed out by Cherayil et al.[11] and Nakamura et al.,[12] however, $A_{2,\Theta}^{(HW)}$ for finite M may possibly remain finite because of three-segment interactions (ternary cluster integral). Very recently, the theory of $A_{2,\Theta}^{(HW)}$ with consideration of three-segment interactions has been presented to show that it may give a rather satisfactory explanation of Monte Carlo (MC) and also previous experimental data.[13] Thus, another purpose of the present paper is to confirm the validity of this theory. We note that the effects of three-segment interactions may be apparently ignored for good-solvent systems.

Experimental Section

Materials. All the a-PαMS samples used in this work are the same as those used in the previous studies[2,3] of α_S, α_η, and α_H, i.e., fractions separated by preparative gel permeation chromatography (GPC) or fractional precipitation from the original samples prepared by living anionic polymerization.[1,14] We note that the sample AMS40 is a fraction from the commercial sample 20538-2 from Polymer Laboratories Ltd. We also note that the initiating chain end of each polymerized sample is a *sec*-butyl group and the other end is a hydrogen atom.

The values of the weight-average molecular weight M_w determined by analytical GPC or from light-scattering (LS) measurements (in cyclohexane at 30.5 °C), the weight-average degree of polymerization x_w estimated from M_w, the ratio of M_w to the number-average molecular weight M_n determined by analytical GPC,[1,2,15] and f_r determined from ^{1}H NMR spectra[1,14,15] are given in Table 1. Although f_r of the samples OAMS5−OAMS10 could not be determined because of the complexity of their ^{1}H NMR spectra, they may be regarded as having almost the same value of f_r as OAMS13, since the samples OAMS5−OAMS13 are fractions from one original

10.1021/ma034481t CCC: $25.00 © 2003 American Chemical Society
Published on Web 06/18/2003

Table 1. Values of M_w, x_w, M_w/M_n, and f_r for Atactic Oligo- and Poly(α-methylstyrene)s

sample	M_w	x_w	M_w/M_n	f_r
OAMS5	6.48×10^2	5	<1.01	
OAMS8	1.04×10^3	8.29	1.01	
OAMS10	1.27×10^3	10.3	1.01	
OAMS13	1.60×10^3	13.1	1.02	0.71
OAMS19	2.27×10^3	18.7	1.07	0.72
OAMS25	2.96×10^3	24.6	1.06	0.72
OAMS33	3.95×10^3	33.0	1.04	0.72
OAMS38	4.57×10^3	38.2	1.07	0.72
OAMS67	7.97×10^3	67.1	1.04	0.72
AMS1	1.30×10^4	109	1.02	0.73
AMS2	2.48×10^4	209	1.02	0.73
AMS5	5.22×10^4	442	1.02	0.73
AMS6	6.46×10^4	547	1.03	0.72
AMS11	1.15×10^5	973	1.04	0.73
AMS15	1.46×10^5	1240	1.02	0.73
AMS24	2.38×10^5	2010	1.05	0.73
AMS40	4.07×10^5	3450	1.02	0.73
AMS80	8.50×10^5	7200	1.05	0.72
AMS200	2.06×10^6	17 400	1.05	0.72
AMS320	3.22×10^6	27 300	1.05	0.73
AMS550	5.46×10^6	46 300		0.70

sample.[14] As seen from the values of f_r, all the samples except AMS550 have the fixed stereochemical composition $f_r = 0.72 \pm 0.01$. Although the value 0.70 of f_r of AMS550 is somewhat smaller than those of the others, this difference may be considered to have no significant effect on solution properties.[2,3] As seen from the values of M_w/M_n, all the samples except AMS550 are very narrow in molecular weight distribution. Although the value of M_w/M_n for the sample AMS550 could not be determined with high accuracy because of the lack of the GPC calibration curve in the necessary range, its molecular weight distribution may be considered to be as narrow as that of the other samples.

The solvents cyclohexane and toluene used for LS measurements were purified according to standard procedures.

Light Scattering. LS measurements were carried out to determine A_2 for the sample OAMS5 in cyclohexane at 30.5 °C (Θ) and for 11 samples with $M_w < 2 \times 10^5$ in toluene at 25.0 °C. For the sample AMS15, the mean-square radius of gyration $\langle S^2 \rangle$ was also determined. Measurements were also made to determine A_2 and $\langle S^2 \rangle$ for the samples AMS40, AMS200, and AMS320 in cyclohexane at 35.0, 45.0, and 55.0 °C. A Fica 50 light-scattering photometer was used for all the measurements with vertically polarized incident light of wavelength 436 nm. For a calibration of the apparatus, the intensity of light scattered from pure benzene was measured at 25.0 °C at a scattering angle of 90°, where the Rayleigh ratio $R_{Uu}(90°)$ of pure benzene was taken as 46.5×10^{-6} cm^{-1}.[16] The depolarization ratio ρ_u of pure benzene at 25.0 °C was determined to be 0.41 ± 0.01 by the method of Rubingh and Yu.[17]

The most concentrated solutions of the samples were prepared gravimetrically and made homogeneous by continuous stirring in the dark at room temperature for 1−3 days in toluene and at ca. 50 °C for 3−7 days in cyclohexane. The solutions were optically purified by filtration through a Teflon membrane of pore size 0.10, 0.45, or 1.0 μm. The solutions of lower concentrations were obtained by successive dilution. The weight fractions of the test solutions were converted to the polymer mass concentrations c by the use of the densities of the respective solutions calculated with the partial specific volumes v_2 of the samples and with the density ρ_0 of the solvent. The quantities v_2 and ρ_0 were measured with a pycnometer of the Lipkin−Davison type having a volume of 10 cm^3.

Scattering data for the excess Rayleigh ratio ΔR_θ as a function of the scattering angle θ and c were analyzed by using the Berry square-root plot[18] for the determination of $\langle S^2 \rangle$, and those for ΔR_0 at $\theta = 0$ as a function of c were analyzed by using the Bawn plot[19] for the determination of A_2. The correction for the anisotropic scattering was then applied to solutions of the samples with $M_w < 4 \times 10^3$.

For a sample with very small M_w, for which the concentration c of its test solution must necessarily be rather high, the dependence on c of the density scattering R_d and of the optical constant K cannot be ignored in the determination of ΔR_0. For the sample OAMS5 with $M_w = 648$, therefore, we adopted the procedure previously[20] presented, which requires experimental values of the reduced total intensity R^*_{Uv} of the unpolarized scattered light for vertically polarized incident light, ρ_u, and the refractive index $\tilde{n}$, all for solutions and the solvent, and also those of the ratio $\kappa_T/\kappa_{T,0}$ of the isothermal compressibility κ_T of a given solution to $\kappa_{T,0}$ of the solvent. We measured R^*_{Uv} and ρ_u, the latter being obtained by the same method as that employed in the calibration of the apparatus. The values of $\tilde{n}$ in each solvent were calculated from

$$\tilde{n} = \tilde{n}_0 + (\partial \tilde{n}/\partial c)_{T,p} c \tag{1}$$

with the values of the refractive index $\tilde{n}_0$ of the solvent and the refractive index increment $(\partial \tilde{n}/\partial c)_{T,p}$, i.e., the partial derivative of $\tilde{n}$ with respect to c at constant temperature T and pressure p (see below). The values of $\kappa_T/\kappa_{T,0}$ are given in the next subsection.

We determined $(\partial \tilde{n}/\partial c)_{T,p}$ as a function of c for each sample at wavelength of 436 nm by the use of a Shimadzu differential refractometer. The values of $(\partial \tilde{n}/\partial c)_{T,p}$ have been found to be independent of c for $c \lesssim 0.15$ g/cm^3. The constant value of $(\partial \tilde{n}/\partial c)_{T,p}$ determined in cyclohexane at Θ is 0.169_4 cm^3/g for the sample OAMS5. Those values in toluene at 25.0 °C are 0.0914_8, 0.102_7, 0.108_3, 0.115_3, 0.120_0, 0.123_1, 0.129_9, and 0.130_2 cm^3/g for the samples OAMS5, OAMS8, OAMS10, OAMS13, OAMS25, OAMS33, OAMS67, and AMS1, respectively, and 0.131 cm^3/g for the samples with $M_w \gtrsim 2 \times 10^4$ independently of M_w. For $\tilde{n}_0$ for pure cyclohexane at 30.5 °C and pure toluene at 25.0 °C, we used the values 1.4298 and 1.5151, respectively. For the samples with $M_w \gtrsim 10^5$ in cyclohexane, $(\partial \tilde{n}/\partial c)_{T,p}$ has been found to be given empirically by

$$(\partial \tilde{n}/\partial c)_{T,p} = 0.190_4 + 4.3_6 \times 10^{-4} T \tag{2}$$

in the range of T from 25.0 to 55.0 °C.

Isothermal Compressibility. Isothermal compressibility measurements were carried out to determine $\kappa_T/\kappa_{T,0}$ for the sample OAMS5 in cyclohexane at Θ and in toluene at 25.0 °C. The apparatus and the method of measurements are the same as those described in the previous paper.[8] The ratio $\kappa_T/\kappa_{T,0}$ was determined as a function of c and pressure p. The pressure p was varied from 1 to ca. 50 atm. This ratio was found to be independent of p within experimental error at any concentration c in this range of p, and therefore, we adopted as its value at 1 atm a mean of values obtained at various pressures. It has then been found that $\kappa_T/\kappa_{T,0}$ for the sample OAMS5 in cyclohexane at Θ and in toluene at 25.0 °C decreases linearly with increasing c as in the cases of a-PS[8] and a- and i-PMMAs.[9,10] The results may be represented by the equation linear in c

$$\kappa_T/\kappa_{T,0} = 1 + kc \tag{3}$$

with $k = -0.75$ and -0.48 cm^3/g in cyclohexane at Θ and in toluene at 25.0 °C, respectively, for $c \lesssim 0.15$ g/cm^3.

Results

Light Scattering. The Berry square-root plot[18] of $(Kc/\Delta R_0)^{1/2}$ against c for each a-PαMS sample neither in cyclohexane at 30.5 °C (Θ) nor in toluene at 25.0 °C has been found to follow a straight line in the range of c studied, although not explicitly shown, indicating that not only the second virial coefficient A'_2 but also the

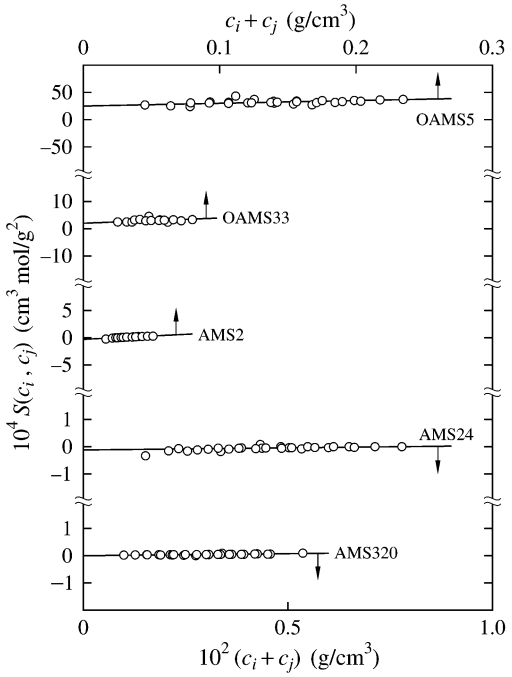

Figure 1. Bawn plots for the indicated a-PαMS samples in cyclohexane at 30.5 °C (Θ).

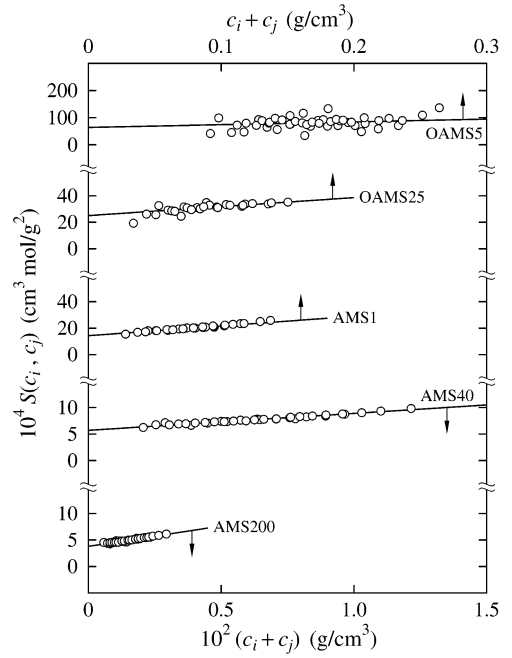

Figure 2. Bawn plots for the indicated a-PαMS samples in toluene at 25.0 °C.

third virial coefficient A'_3 contributes to $Kc/\Delta R_0$ as c is increased. (Here, the prime attached to A_2 and A_3 indicates that they are *light-scattering* virial coefficients.[9,20]) We note that the data points for each sample in cyclohexane follow a curve concave upward, while those in toluene follow a curve concave upward or downward, depending on M_w, indicating that the so-called g factor defined by $A'_3/A'^2_2 M_w$ in toluene is not always larger than $^1/_3$.[5] It is then difficult to determine A'_2 from the plot with high accuracy, so that we have made the Bawn plot.[19]

Figures 1 and 2 show the Bawn plots for the indicated a-PαMS samples in cyclohexane at 30.5 °C and in toluene at 25.0 °C, respectively, where $S(c_i, c_j)$ is defined by

$$S(c_i, c_j) \equiv [(Kc/\Delta R_0)_{c=c_j} - (Kc/\Delta R_0)_{c=c_i}]/(c_j - c_i)$$
$$= 2A'_2 + 3A'_3(c_i + c_j) + \ldots \quad (4)$$

We note that the Bawn plots for the samples except OAMS5 in cyclohexane and for the samples with $M_w > 2 \times 10^5$ in toluene have been made by the use of previous LS data for ΔR_0.[1,2,15] As seen from the figures, the data points for each sample in each solvent follow a straight line, although those for the sample OAMS5 in toluene are somewhat scattered. These results indicate that the terms higher than A'_3 may be neglected in the range of c studied. From the straight lines indicated, we have determined A'_2 and A'_3 for each sample in each solvent. Then we have determined M_w for the sample OAMS5 in cyclohexane at 30.5 °C and for the samples OAMS5 through AMS15 in toluene 25.0 °C so that the curve of $(Kc/\Delta R_0)^{1/2}$ calculated by the use of these values of M_w, A'_2, and A'_3 gives a best fit to the data points for each sample in each solvent in the Berry square-root plot. The values of A'_2 and A'_3 have been similarly determined for the samples AMS40, AMS200, and AMS320 in cyclohexane at 35.0, 45.0, and 55.0 °C and for the samples with $M_w > 2 \times 10^5$ in 4-*tert*-butyltoluene at 25.0 °C and in *n*-butyl chloride at 25.0 °C, although not explicitly shown here, where we have used LS data for ΔR_0 previously[2] obtained in the latter two solvents. For the samples AMS40, AMS200, and AMS320 in cyclohexane at 35.0, 45.0, and 55.0 °C, we have also determined $\langle S^2 \rangle$ from the Berry square-root plots.

The values of A'_2 and A'_3 so determined for each a-PαMS sample in each solvent may be equated to those of the (osmotic) second and third virial coefficients A_2 and A_3, respectively, as in the previous cases of a-PS[8] and a- and i-PMMAs.[9,10] We treat only the results for A_2 in the remainder of this paper, and we will analyze those for A_3 in a forthcoming paper.

Second Virial Coeffcient. The values of A_2 so determined for the a-PαMS samples in cyclohexane at 30.5 °C (Θ), in toluene at 25.0 °C, in 4-*tert*-butyltoluene at 25.0 °C, and in *n*-butyl chloride at 25.0 °C are given in the third, fifth, seventh, and ninth columns, respectively, of Table 2 along with those of M_w. The values of M_w for the samples OAMS8 through AMS550 in cyclohexane and those for the samples AMS24 through AMS550 in the three other solvents have been reproduced from refs 1, 2, and 15. In Table 3 are given the values of A_2 for the samples AMS40, AMS200, and AMS320 in cyclohexane at 35.0, 45.0, and 55.0 °C along with those of $\langle S^2 \rangle^{1/2}$. The values of M_w in the second column of Table 3 have been reproduced from the second column of Table 2.

Figure 3 shows plots of $A_{2,\Theta}$ against $\log M_w$ in cyclohexane at 30.5 °C (Θ). In the figure, the solid, dashed, and dotted curves represent the theoretical values of $A_{2,\Theta}$ $(=A_{2,\Theta}^{(HW)} + A_2^{(E)})$, $A_{2,\Theta}^{(HW)}$, and $A_2^{(E)}$, respectively, which are obtained and discussed in the next (Discussion) section. As M_w is decreased, $A_{2,\Theta}$ first decreases slowly from zero to a negative minimum in the range of $M_w \gtrsim 5 \times 10^4$ and then increases rather steeply. The sharp increase in $A_{2,\Theta}$ for small M_w is due to the effects of chain ends[4,6] as in the cases of a-PS in cyclohexane at 34.5 °C (Θ)[21] and a-PMMA in acetonitrile at 44.0 °C (Θ).[4,9] However, the value of $A_{2,\Theta}$ for a-PαMS remains definitely negative even for such large M_w ($\gtrsim 10^5$) where

Table 2. Results of LS Measurements for Atactic Oligo- and Poly(α-methylstyrene)s in Θ and Good Solvents

	cyclohexane, 30.5 °C (Θ)		toluene, 25.0 °C		4-*tert*-butyltoluene, 25.0 °C		*n*-butyl chloride, 25.0 °C	
sample	$10^{-4}M_w$	10^4A_2, cm^3 mol/g^2	$10^{-4}M_w$	10^4A_2, cm^3 mol/g^2	$10^{-4}M_w$	10^4A_2, cm^3 mol/g^2	$10^{-4}M_w$	10^4A_2, cm^3 mol/g^2
OAMS5	0.064_8	12.5	0.064_6	32.0				
OAMS8	0.104[a]	7.20[b]	0.105	24.6				
OAMS10	0.127	5.60	0.128	19.7				
OAMS13	0.160	4.00	0.162	18.8				
OAMS19	0.227	2.35						
OAMS25	0.296	1.75	0.304	12.5				
OAMS33	0.395	1.00	0.399	10.9				
OAMS38	0.457	0.55						
OAMS67	0.797	0.30	0.82	8.30				
AMS1	1.30	0.08	1.34	7.15				
AMS2	2.48	−0.15	2.53	5.85				
AMS5	5.22	−0.28	5.39	4.73				
AMS6	6.46	−0.26						
AMS11	11.5	−0.12						
AMS15	14.6	−0.15	15.0	3.58				
AMS24	23.8	−0.06	24.3[c]	3.15[d]	23.7[c]	1.38[d]	24.3[c]	1.09[d]
AMS40	40.7	0	40.7	2.85	40.8	1.21	41.0	0.98
AMS80	85.0	0	87.7	2.28	86.2	1.01	85.3	0.82
AMS200	206	0	203	1.90	200	0.86	204	0.70
AMS320	322	0	324	1.65	316	0.79	320	0.60
AMS550	546	0	556	1.45	556	0.67	547	0.52

[a] M_w's for OAMS8 through AMS550 in cyclohexane have been reproduced from refs 1, 2, and 15. [b] A_2's for OAMS8 through AMS550 in cyclohexane have been determined from LS data for ΔR_0 obtained in refs 1, 2, and 15. [c] M_w's for AMS24 through AMS550 in toluene, 4-*tert*-butyltoluene, and *n*-butyl chloride are from ref 2. [d] A_2's for AMS24 through AMS550 in toluene, 4-*tert*-butyltoluene, and *n*-butyl chloride have been determined from LS data for ΔR_0 obtained in ref 2.

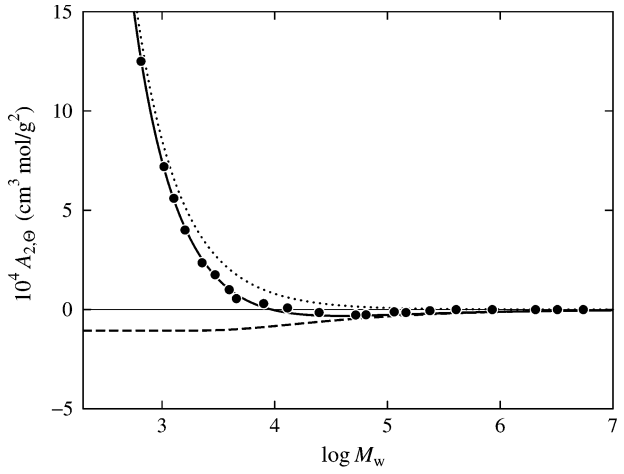

Figure 3. Plots of $A_{2,\Theta}$ against log M_w for a-PαMS in cyclohexane at 30.5 °C (Θ). The solid, dashed, and dotted curves represent the theoretical values of $A_{2,\Theta}$ ($=A_{2,\Theta}^{(HW)} + A_2^{(E)}$), $A_{2,\Theta}^{(HW)}$, and $A_2^{(E)}$, respectively (see the text).

Table 3. Results of LS Measurements for Atactic Poly(α-methylstyrene) in Cyclohexane at 35.0, 45.0, and 55.0 °C

		35.0 °C		45.0 °C		55.0 °C	
sample	$10^{-4}M_w$	$\langle S^2\rangle^{1/2}$, Å	10^4A_2, cm^3 mol/g^2	$\langle S^2\rangle^{1/2}$, Å	10^4A_2, cm^3 mol/g^2	$\langle S^2\rangle^{1/2}$, Å	10^4A_2, cm^3 mol/g^2
AMS40	40.7	172	0.20	179	0.55	186	0.80
AMS200	206	404	0.18	437	0.41	462	0.58
AMS320	322	508	0.17	558	0.37	595	0.52

the effects of chain ends may be considered to be negligibly small, as in the case of a-PS in *trans*-decalin at 21.0 °C (Θ).[22] This may be regarded as arising from possible effects of three-segment interactions.[12,13] Such behavior of $A_{2,\Theta}$ for a-PαMS in the range of M_w displayed is quite similar to that for the MC chains very recently studied (see Figures 6 and 11 of ref 13).

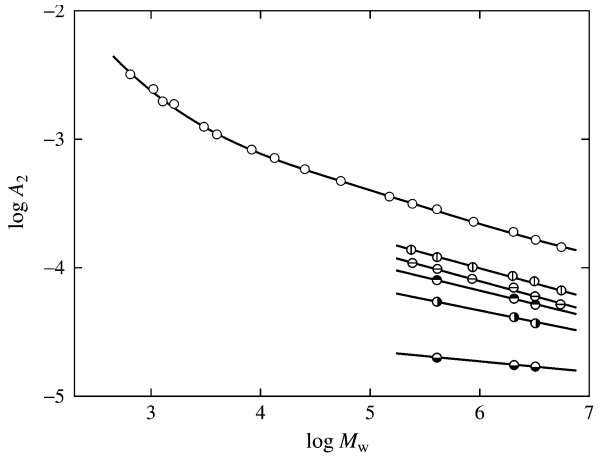

Figure 4. Double-logarithmic plots of A_2 (in cm^3 mol/g^2) against M_w for a-PαMS: (○) in toluene at 25.0 °C; (◐) in 4-*tert*-butyltoluene at 25.0 °C; (⊖) in *n*-butyl chloride at 25.0 °C; (◓) in cyclohexane at 55.0 °C; (◑) in cyclohexane at 45.0 °C; (◒) in cyclohexane at 35.0 °C. The solid curve connects smoothly the data points in each solvent.

Figure 4 shows double-logarithmic plots of A_2 (in cm^3 mol/g^2) against M_w in toluene at 25.0 °C (unfilled circles), in 4-*tert*-butyltoluene at 25.0 °C (circles with vertical bar), in *n*-butyl chloride at 25.0 °C (circles with horizontal bar), and in cyclohexane at 55.0 °C (top-half-filled circles), 45.0 °C (right-half-filled circles), and 35.0 °C (bottom-half-filled circles). The solid curve connects smoothly the data points in each solvent. It is seen that A_2 in toluene exhibits an upswing with decreasing M_w for small M_w. This sharp increase in A_2 in toluene is also due to the effects of chain ends[4,6] as in the cases of a-PS in toluene at 15.0 °C and a- and i-PMMAs in acetone at 25.0 °C.[4,8−10]

Discussion

HW Theory. We begin by summarizing basic equations in the HW theory[4,6,13] necessary for an analysis of the experimental data for A_2 given in the last (Results)

section. The theory takes account of both effects of chain stiffness and chain ends, and also of those of three-segment interactions at the Θ temperature, the last of which have very recently been considered,[13] on the basis of the HW touched-bead model (with excluded volume). The model is such that $n + 1$ beads are arrayed with spacing a between them along the contour of total length $L = na$, where $n - 1$ intermediate beads are identical and the two end beads are different from the intermediate ones and also from each other in species. Identical excluded-volume interactions between intermediate beads are expressed in terms of the *effective* binary-cluster integral β, which is redefined so as to include the contribution of three-segment interactions (ternary cluster integral).[4,13,23] In addition to β, two kinds of excess binary-cluster integrals β_1 and β_2 are introduced to express interactions between unlike (and like end) beads, β_1 being associated with one end bead and β_2 with two end ones. The HW model itself[4] is defined in terms of three basic model parameters: the constant differential-geometrical curvature κ_0 and torsion τ_0 of its characteristic helix and the static stiffness parameter λ^{-1}.

According to the theory,[4,6] A_2 may be written as

$$A_2 = A_2^{(\mathrm{HW})} + A_2^{(\mathrm{E})} \tag{5}$$

where $A_2^{(\mathrm{HW})}$ is the part of A_2 (arising from β) without the effects of chain ends, and $A_2^{(\mathrm{E})}$ represents their contribution to A_2 (from β_1 and β_2). The first term $A_2^{(\mathrm{HW})}$ at $\beta \neq 0$ may be given by

$$A_2^{(\mathrm{HW})} = (N_\mathrm{A} {c_\infty}^{3/2} L^2 B/2M^2) h(\hat{z}) \tag{6}$$

where N_A is the Avogadro constant, and the constant c_∞ and the excluded-volume strength B are defined by

$$c_\infty = \lim_{\lambda L \to \infty} (6\lambda \langle S^2 \rangle_0 / L) = [4 + (\lambda^{-1}\tau_0)^2]/[4 + (\lambda^{-1}\kappa_0)^2 + (\lambda^{-1}\tau_0)^2] \tag{7}$$

and

$$B = \beta / a^2 {c_\infty}^{3/2} \tag{8}$$

The so-called h function in eq 6 is given by

$$h(\hat{z}) = (1 + 7.74\hat{z} + 52.3\hat{z}^{27/10})^{-10/27} \tag{9}$$

with

$$\hat{z} = \tilde{\tilde{z}} / {\alpha_\mathrm{S}}^3 \tag{10}$$

In eq 10, $\tilde{\tilde{z}}$ is the intermolecular scaled excluded-volume parameter defined by

$$\tilde{\tilde{z}} = [Q(\lambda L)/2.865] z \tag{11}$$

where the coefficient $Q(L)$ as a function of (reduced) L represents the effects of chain stiffness on the intermolecular excluded-volume effect, as explicitly given below, and the conventional excluded-volume parameter[5] z is defined by

$$z = (3/2\pi)^{3/2} (\lambda B)(\lambda L)^{1/2} \tag{12}$$

According to the QTP scheme or the Yamakawa–Stockmayer–Shimada theory,[4,24–26] α_S in eq 10 may be given by the Domb–Barrett equation[27]

$${\alpha_\mathrm{S}}^2 = [1 + 10\tilde{z} + (70\pi/9 + 10/3)\tilde{z}^2 + 8\pi^{3/2}\tilde{z}^3]^{2/15} \times [0.933 + 0.067 \exp(-0.85\tilde{z} - 1.39\tilde{z}^2)] \tag{13}$$

with the intramolecular scaled excluded-volume parameter $\tilde{z}$ defined by

$$\tilde{z} = {}^3/_4 K(\lambda L) z \tag{14}$$

in place of z. In eq 14, the coefficient $K(L)$ as a function of (reduced) L represents the effects of chain stiffness on the intramolecular excluded-volume effect and is given by

$$K(L) = \frac{4}{3} - 2.711 L^{-1/2} + \frac{7}{6} L^{-1} \text{ for } L > 6$$
$$= L^{-1/2} \exp(-6.611 L^{-1} + 0.9198 + 0.03516 L) \text{ for } L \leq 6 \tag{15}$$

The coefficient $Q(L)$ in eq 11 is given in a very good approximation for (reduced) $L \gtrsim 1$ by[4,6]

$$Q(L) = -\frac{128\sqrt{2}}{15} - 2.531 L^{-1/2} - 2.586 L^{-1} + 1.985 L^{-3/2} - 1.984 L^{-2} - 0.9292 L^{-5/2} + 0.1223 L^{-3} + \frac{8}{5} x^{5/2} + \frac{2}{3} x^{3/2} \left(8 + \frac{1}{6} L^{-1}\right) + x^{1/2}(8 - 13.53 L^{-1} + 0.2804 L^{-2}) - x^{-1/2} L^{-1} (0.3333 - 5.724 L^{-1} + 0.7974 L^{-2}) - x^{-3/2} L^{-2} (0.3398 - 0.7146 L^{-1}) \tag{16}$$

with

$$x = 1 + 0.961 L^{-1} \tag{17}$$

We simply put $h = 1$ (rod limit) for $\lambda L \lesssim 1$, in which range eq 16 is not valid. We note that L is related to M by the equation

$$L = M / M_\mathrm{L} \tag{18}$$

with M_L being the shift factor as defined as the molecular weight per unit contour length.

The first term on the right-hand side of eq 5 at the Θ temperature ($\beta = 0$), which we denote by $A_{2,\Theta}^{(\mathrm{HW})}$, may be given by[13]

$$A_{2,\Theta}^{(\mathrm{HW})} = -\frac{3 {A_3}^0 (\lambda / M_\mathrm{L})^{1/2}}{8\pi^{3/2} N_\mathrm{A} (\langle S^2 \rangle_0 / M)_\infty^{3/2}} [I(\infty) - I(\lambda L)] \tag{19}$$

where ${A_3}^0$ is the third virial coefficient without the effects of chain ends at the Θ temperature,[4,28] $(\langle S^2 \rangle_0 / M)_\infty$ is the value of $\langle S^2 \rangle_0 / M$ in the limit of $M \to \infty$, and

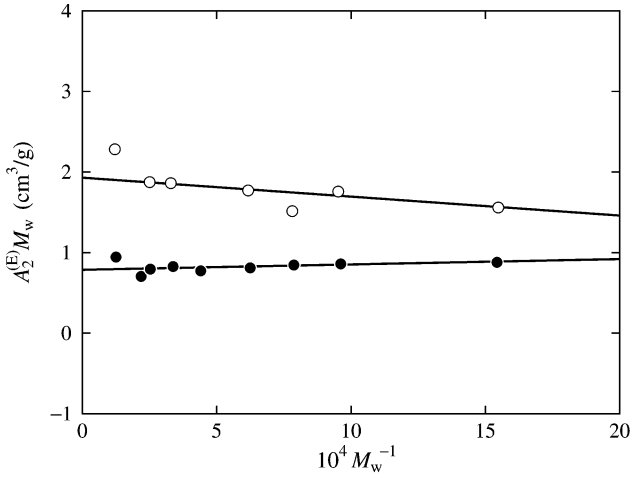

Figure 5. Plots of $A_2^{(E)}M_w$ against M_w^{-1} for a-PαMS. The symbols have the same meaning as those in Figures 3 and 4.

the function $I(L)$ of (reduced) L is given by

$$I(L) = \exp(-6L^{-1} + 0.3472 - 0.087L) \quad \text{for } 0 \le L \le 3.075$$

$$= 0.4149 - 0.8027L^{-1} + 0.01L^{-1}(7.132\Delta^2 - 0.9315\Delta^3 + 0.1057\Delta^4 - 0.005745\Delta^5) \quad \text{for } 3.075 < L < 7.075$$

$$= 1.465 - 4L^{-1/2} + 3.476L^{-1} - \frac{5}{6}L^{-3/2} \quad \text{for } 7.075 \le L \quad (20)$$

with $\Delta = L - 3.075$. The term $A_{2,\Theta}^{(HW)}$ remains small but finite negative even at $\beta = 0$ because of the residual contribution of three-segment interactions, which cannot be absorbed into β. We note that $A_{2,\Theta}^{(HW)} \propto M^{-1/2}$ for large M, and that this residual contribution may be ignored for good-solvent systems since the ternary cluster integral (>0) may decrease with increasing solvent power above the Θ temperature.[13]

The second term $A_2^{(E)}$ on the right-hand side of eq 5 may be written in the form[4, 6]

$$A_2^{(E)} = a_1M^{-1} + a_2M^{-2} \quad (21)$$

where

$$a_1 = 2N_A\beta_1/M_0$$
$$a_2 = 2N_A\Delta\beta_2 \quad (22)$$

with M_0 the molecular weight of the bead and with

$$\Delta\beta_2 = \beta_2 - 2\beta_1 \quad (23)$$

The excess binary-cluster integrals β_1 and β_2 are explicitly defined in eqs 8.117 of ref 4, where the symbols $\beta_{2,1}$ and $\beta_{2,2}$ are used in place of β_1 and β_2, respectively.

Effects of Chain Ends and Three-Segment Interactions. Now we analyze the data for A_2 given in Table 2 by the use of the above theory. First, for convenience, we examine the effects of chain ends and three-segment interactions, the latter applying only to $A_{2,\Theta}$. In Figure 5, the values of $A_2^{(E)}M_w$ are plotted against M_w^{-1} on the basis of eq 21 for the samples with $M_w < 10^4$ in cyclohexane at 30.5 °C (filled circles) and in toluene at 25.0 °C (unfilled circles) in order to determine a_1 and a_2 (and hence β_1 and β_2) from the intercept and slope, respectively. We have evaluated $A_2^{(E)}$ for each of the nine a-PαMS samples in cyclohexane by subtracting the theoretical value of $A_{2,\Theta}^{(HW)}$ from the observed value of A_2, the former value being calculated from eq 19 with eqs 18 and 20 with the respective values of 46.8 Å and 39.8 Å^{-1} of λ^{-1} and M_L previously[1] determined from $\langle S^2\rangle_0$ and the respective observed values 6.82×10^{-18} cm^2 and 5.0×10^{-4} cm^6 mol/g^3 of $(\langle S^2\rangle_0/M_w)_\infty$ and $A_3{}^0$. We note that the value of $(\langle S^2\rangle_0/M_w)_\infty$ has been determined in the previous paper[1] and that the value of $A_3{}^0$ has been evaluated as a mean of values of A_3 for the six samples AMS24 through AMS550, for which the effects of chain ends are negligibly small, although not explicitly given here. Similarly, we have evaluated $A_2^{(E)}$ for each of the seven a-PαMS samples in toluene by the use of the theoretical value of $A_2^{(HW)}$ calculated from eq 6 with eqs 7−18 (assuming that $h = 1$ for $\lambda L \lesssim 1$) with the above-mentioned values of λ^{-1} and M_L along with the respective values[1] 3.0 and 0.9 of $\lambda^{-1}\kappa_0$ and $\lambda^{-1}\tau_0$ and the value 0.43 of λB.[2]

It is seen from Figure 5 that the data points in each solvent can be fitted by a straight line, confirming the validity of eq 21. From the straight lines, a_1 and a_2 are found to be 0.79 cm^3/g and 67 cm^3/mol, respectively, in cyclohexane at 30.5 °C, and 1.9 cm^3/g and −240 cm^3/mol, respectively, in toluene at 25.0 °C. From eqs 22 and 23 with the values of a_1 and a_2 so obtained, β_1 and β_2 are calculated to be 77 and 210 Å^3, respectively, in cyclohexane at 30.5 °C, and 190 and 180 Å^3, respectively, in toluene at 25.0 °C, where we have taken the repeat unit of the chain as a single bead ($M_0 = 118$). These values of β_1 and β_2 in toluene are comparable to those obtained for a-PS in the same solvent.[8]

The solid, dashed, and dotted curves in Figure 3 represent the theoretical values of $A_{2,\Theta}$ ($= A_{2,\Theta}^{(HW)} + A_2^{(E)}$), $A_{2,\Theta}^{(HW)}$, and $A_2^{(E)}$, respectively. The values of $A_{2,\Theta}^{(HW)}$ have been calculated as mentioned above, and those of $A_2^{(E)}$ have been calculated from eq 21 with the above-determined values of a_1 and a_2 in cyclohexane at 30.5 °C. All the data points follow closely the solid curve as a whole, although strictly, the observed $A_{2,\Theta}$ becomes 0 somewhat faster than the theoretical one as M_w is increased. It is clearly seen that the sharp increase in $A_{2,\Theta}$ with decreasing M_w for small M_w arises from that in $A_2^{(E)}$, while the rather long-tailed negative values of $A_{2,\Theta}$ for large M_w arises from $A_{2,\Theta}^{(HW)}$, i.e., the residual contribution of three-segment interactions.

Figure 6 shows a comparison of the present data for $A_{2,\Theta}$ for a-PαMS in cyclohexane at 30.5 °C (Θ) with previous ones for a-PS in cyclohexane at 34.5 °C (Θ)[8,21] and a-PMMA in acetonitrile at 44.0 °C (Θ).[9,29] The filled circles, squares, and triangles represent the experimental values of $A_{2,\Theta}$ for a-PαMS, a-PS, and a-PMMA, respectively, and the solid, dashed, and dot−dashed curves the respective theoretical ones. The theoretical values for a-PαMS have been reproduced from Figure 3 and those for a-PS and a-PMMA from ref 13. We note that these theoretical values of $A_{2,\Theta}$ for a-PS and a-PMMA are different from the original ones[4,8,9] and have been recalculated from eq 5 with $A_{2,\Theta}^{(HW)}$ given by eq 19 with eq 20 in place of $A_2^{(HW)}$ and with eqs 18 and 21−23 with the values of the HW model parameters λ^{-1} (in Å) and M_L (in Å^{-1}), which are 20.6 and 35.8,

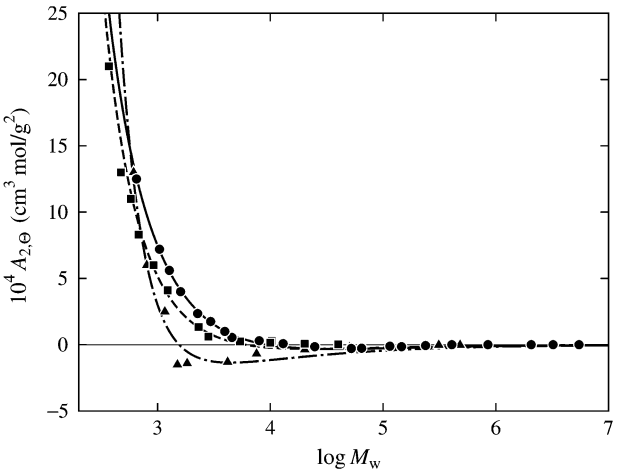

Figure 6. Plots of $A_{2,\Theta}$ against logM_w: (●) present data for a-PαMS in cyclohexane at 30.5 °C (Θ); (■) a-PS in cyclohexane at 34.5 °C (Θ);[8,21] (▲) a-PMMA in acetonitrile at 44.0 °C (Θ).[9,29] The solid, dashed, and dot−dashed curves represent the theoretical values of $A_{2,\Theta}$ ($=A_{2,\Theta}^{(HW)} + A_2^{(E)}$) for a-PαMS, a-PS, and a-PMMA, respectively (see the text).

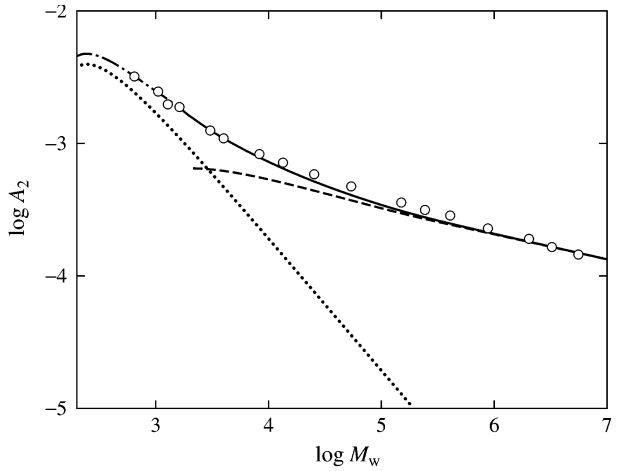

Figure 7. Double-logarithmic plots of A_2 (in cm^3 mol/g^2) against M_w for a-PαMS in toluene at 25.0 °C. The solid and dot−dashed curves represent the theoretical values of A_2 ($= A_2^{(HW)} + A_2^{(E)}$), and the dashed and dotted curves those of $A_2^{(HW)}$ and $A_2^{(E)}$, respectively (see the text).

respectively, for a-PS,[4,30] and 57.9 and 36.3, respectively, for a-PMMA,[4,31] and also with the values of $A_3{}^0$ (in cm^6 mol/g^3) and $(\langle S^2\rangle_0/M)_\infty$ (in cm^2 mol/g), which are 4.7×10^{-4} and $7.8_2 \times 10^{-18}$, respectively, for a-PS,[28,30] and 5.8×10^{-4} and $6.5_7 \times 10^{-18}$, respectively, for a-PMMA.[28,31] We also note that the values of β_1 and β_2 determined in ref 13 are 44 and 200 Å^3, respectively, for a-PS, and −19 and 500 Å^3, respectively, for a-PMMA. These values of β_1 and β_2 for a-PS in cyclohexane are comparable to the above-determined corresponding values for a-PαMS in the same solvent. It is seen that all the data points for a-PS and a-PMMA follow closely the respective theoretical (dashed and dot−dashed) curves as a whole as in the case of a-PαMS, although strictly, they deviate slightly upward from the respective theoretical curves in the range of $10^4 \lesssim M \lesssim 10^5$.

Figure 7 shows double-logarithmic plots of A_2 (in cm^3 mol/g^2) against M_w for a-PαMS in toluene at 25.0 °C. The solid curve represents the theoretical values calculated from eq 5 (for $\lambda L \gtrsim 1$), and the dot−dashed curve those from eq 5 with eq 6 with $h = 1$ (for $\lambda L \lesssim 1$). The contributions of $A_2^{(HW)}$ (for $\lambda L \gtrsim 1$) and $A_2^{(E)}$ are shown by the dashed and dotted curves, respectively, where the former has been calculated from eq 6 with eqs 7−18 with the above-given values of the HW model parameters, and the latter from eq 21 with the above-determined values of a_1 and a_2. Agreement between theory and experiment is seen to be rather satisfactory, although strictly, the theoretical values are slightly smaller than the experimental ones in the range of $2 \times 10^4 \lesssim M_w \lesssim 5 \times 10^5$.

Finally, we note that for $\langle S^2\rangle$ and α_S, the effects of chain ends may be ignored[32] and the residual contribution of three-segment interactions may be absorbed into the HW model parameters and β.[13]

Interpenetration Function. Next we examine the effects of chain stiffness on the (true) interpenetration function Ψ, which is defined for $A_2^{(HW)}$ without the effects of chain ends as follows[4,8]

$$\Psi = A_2^{(HW)} M^2/4\pi^{3/2} N_A \langle S^2\rangle^{3/2} \tag{24}$$

Substitution of eq 6 into eq 24 leads to the HW theory expression[4,8]

$$\Psi = (6\lambda\langle S^2\rangle_0/c_\infty L)^{-3/2} \bar{z} h(\hat{z}) \tag{25}$$

with

$$\bar{z} = z/\alpha_S^3 \tag{26}$$

In the coil limit ($M \to \infty$ or $\lambda L \to \infty$), we have $\tilde{z} = \tilde{\tilde{z}} = z$ and $6\lambda\langle S^2\rangle_0/c_\infty L = 1$, so that eq 25 reduces to the TP theory expression[4,5]

$$\Psi = \bar{z} h(z) \tag{27}$$

where $h(z)$ is given by eq 9 with $\hat{z} = \bar{z}$. For comparison, we also consider the *apparent* interpenetration function Ψ_{ap},[8] which is defined from the whole A_2 with the contribution $A_2^{(E)}$ of the effects of chain ends as follows

$$\Psi_{ap} = A_2 M^2/4\pi^{3/2} N_A \langle S^2\rangle^{3/2} \tag{28}$$

Recall that this is the usual definition of the interpenetration function,[5] and note that necessarily, Ψ and Ψ_{ap} become identical to each other for such large M where $A_2^{(E)}$ may be neglected.

In Table 4 are given the values of Ψ and Ψ_{ap} for a-PαMS in toluene at 25.0 °C and those of Ψ in 4-*tert*-butyltoluene at 25.0 °C and in *n*-butyl chloride at 25.0 °C along with those of $\alpha_S{}^3$. We have calculated the values of Ψ_{ap} in toluene at 25.0 °C from eq 28 with the values of A_2 and M_w given in Table 2 and those of $\langle S^2\rangle^{1/2}$ given in Table 2 of ref 2 for the samples except OAMS5 and AMS15. For $\langle S^2\rangle^{1/2}$ for the samples OAMS5 and AMS15, we have assumed the value 4.0_1 Å previously determined for the former in cyclohexane at 30.5 °C (Θ)[1] since the intramolecular excluded-volume effect may be ignored for it, and used the value $1.3_0 \times 10^2$ Å determined for the latter in the present study. We have also calculated the value of Ψ for each a-PαMS sample in toluene at 25.0 °C from eq 24 with the above-mentioned values of M_w and $\langle S^2\rangle^{1/2}$ and the value of $A_2^{(HW)}$ obtained from the value of A_2 given in Table 2 by subtraction of the value of $A_2^{(E)}$ calculated from eq 21 with the values of a_1 and a_2 determined in the last subsection. From the values of Ψ and Ψ_{ap} so obtained, it is seen that the difference between them (due to $A_2^{(E)}$) decreases with

Table 4. Values of Ψ (Ψ_{ap}) and α_S^3 for Atactic Oligo- and Poly(α-methylstyrene)s in Toluene at 25.0 °C, in 4-*tert*-Butyltoluene at 25.0 °C, and in *n*-Butyl Chloride at 25.0 °C

	toluene, 25.0 °C		4-*tert*-butyltoluene, 25.0 °C		*n*-butyl chloride, 25.0 °C	
sample	Ψ (Ψ_{ap})	α_S^3	Ψ	α_S^3	Ψ	α_S^3
OAMS5	0.374 (1.54)	1[a]				
OAMS8	0.274 (0.801)	1				
OAMS10	0.173 (0.564)	1				
OAMS13	0.197 (0.473)	1.00[b]				
OAMS25	0.164 (0.320)	1.02				
OAMS33	0.167 (0.293)	1.03				
OAMS67	0.211 (0.292)	1.12				
AMS1	0.229 (0.286)	1.23				
AMS2	0.251 (0.289)	1.41				
AMS5	0.252 (0.273)	1.73				
AMS15	0.261 (0.270)	2.22				
AMS24	0.252 (0.259)	2.54	0.182	1.49	0.164	1.37
AMS40	0.244 (0.248)	3.11	0.203	1.63	0.174	1.55
AMS80	0.244 (0.246)	3.81	0.206	1.94	0.188	1.69
AMS200	0.233 (0.235)	4.69	0.211	2.30	0.201	2.02
AMS320	0.226 (0.227)	5.67	0.212	2.74	0.201	2.26
AMS550	0.225 (0.226)	6.60	0.213	3.19	0.207	2.48

[a] The values of α_S^3 for OAMS5, OAMS8, and OAMS10 have been assumed to be 1. [b] The values of α_S^3 are from ref 2 except for OAMS5, OAMS8, OAMS10, and AMS15 (present work).

Table 5. Values of Ψ and α_3^S for Atactic Poly(α-methylstyrene) in Cyclohexane at 35.0, 45.0, and 55.0 °C

	35.0 °C		45.0 °C		55.0 °C	
sample	Ψ	α_S^3	Ψ	α_S^3	Ψ	α_S^3
AMS40	0.049	1.11	0.117	1.26	0.152	1.42
AMS200	0.084	1.24	0.157	1.57	0.184	1.86
AMS320	0.100	1.30	0.165	1.72	0.189	2.09

increasing M_w and may be neglected for the samples AMS24 through AMS550, so that we have assumed that $\Psi = \Psi_{ap}$ for these samples also in 4-*tert*-butyltoluene at 25.0 °C and in *n*-butyl chloride at 25.0 °C, and calculated the values of Ψ from eq 28 with the values of A_2 and M_w given in Table 2 and those of $\langle S^2\rangle^{1/2}$ given in Table 2 of ref 2. The values of α_S^3 in Table 4 have been reproduced from Table 3 of ref 2 for the samples except OAMS5, OAMS8, OAMS10, and AMS15 in toluene at 25.0 °C. We have assumed that $\alpha_S^3 = 1$ for the samples OAMS5, OAMS8, and OAMS10 in toluene at 25.0 °C. For the evaluation of α_S^3 for the sample AMS15 in toluene at 25.0 °C, we have used the above-mentioned value of $\langle S^2\rangle^{1/2}$ and adopted as $\langle S^2\rangle_0^{1/2}$ the value 99.$_9$ Å of $\langle S^2\rangle_\Theta^{1/2}$ estimated from the experimental relation $(\langle S^2\rangle_\Theta/M_w)_\infty = 6.82\times10^{-18}$ cm^2 previously obtained in cyclohexane at Θ.[1]

The values of Ψ and α_S^3 for the samples AMS40, AMS200, and AMS320 in cyclohexane at 35.0, 45.0, and 55.0 °C are given in Table 5. As seen from Figure 3, $A_2^{(E)}$ for these samples may be neglected (i.e., $\Psi = \Psi_{ap}$), so that we have calculated the values of Ψ from eq 28 with the values of A_2, M_w, and $\langle S^2\rangle^{1/2}$ given in Table 3. In the evaluation of α_S^3 for them, we have used the values of $\langle S^2\rangle^{1/2}$ given in Table 3 and those of $\langle S^2\rangle_\Theta^{1/2}$ in cyclohexane at Θ given in Table 3 of ref 1.

Figure 8 shows plots of Ψ so evaluated against α_S^3 for a-PαMS in toluene at 25.0 °C, in 4-*tert*-butyltoluene at 25.0 °C, in *n*-butyl chloride at 25.0 °C, and in cyclohexane at 35.0, 45.0, and 55.0 °C in the range of $\lambda L \gtrsim 1$ ($M_w \gtrsim 2 \times 10^3$). In the figure, various types of

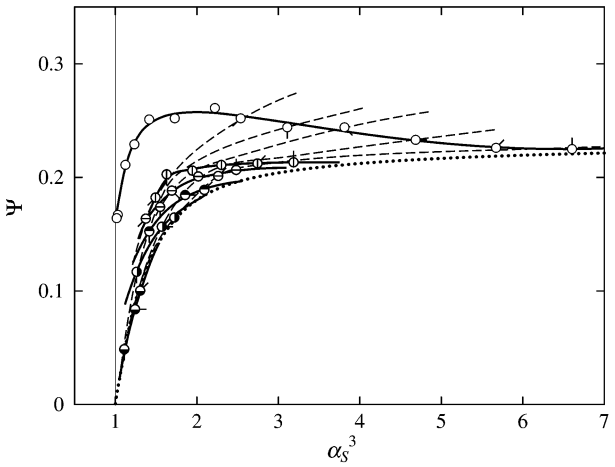

Figure 8. Plots of Ψ against α_S^3 for a-PαMS. Various types of circles have the same meaning as those in Figure 4. Various directions of pips indicate different values of M_w of the six highest-molecular-weight samples: pip up, AMS550; pip right-up, AMS320; pip right, AMS200; pip right-down, AMS80; pip down, AMS40; pip left-down, AMS24. The solid and dashed curves connect smoothly the data points at constant *B* (solvent condition) and M_w, respectively. The dotted curve represents the TP theory values.

circles have the same meaning as those in Figure 4, indicating different solvent conditions (different excluded-volume strengths *B*), and various directions of pips attached to the circles for the six samples with the highest M_w indicate different values of M_w. The solid and dashed curves connect smoothly the data points at constant *B* and M_w, respectively. The dotted curve represents the TP theory values calculated from eq 27 with eqs 9, 13, and 26 with $\tilde{z} = \tilde{\tilde{z}} = z$. As in the previous cases of a-PS ($f_r = 0.59$),[4,7,8] a-PMMA ($f_r = 0.79$),[4,9] and i-PMMA ($f_r \simeq 0.01$),[10] Ψ as a function of α_S^3 depends separately on M_w and *B* and deviates appreciably upward from the TP theory prediction, reconfirming that neither the TP nor the QTP theory can explain the behavior of Ψ. Specifically, as α_S^3 (or *M*) is decreased, Ψ in toluene increases for $\alpha_S^3 \gtrsim 3$, then passes through a flat hump at $\alpha_S^3 \simeq 2$, and finally decreases. On the other hand, Ψ in 4-*tert*-butyltoluene, in *n*-butyl chloride, and in cyclohexane above Θ decreases monotonically with decreasing α_S^3. As shown by the dashed curves, Ψ increases more rapidly than the TP theory prediction and with larger slopes for smaller M_w as α_S^3 (or *B*) is increased at constant M_w.

As for the behavior of Ψ for a-PαMS in toluene at 25.0 °C, it is pertinent to make here some comments on literature data. As pointed out long ago,[33] the values of Ψ obtained by Kato et al.[34] for a-PαMS in the same solvent condition are only about 0.19 in the range of $4 \lesssim \alpha_S^3 \lesssim 5$ and are appreciably smaller than the present value nearly equal to 0.23. This difference may be regarded as arising mainly from the fact that their values of $\langle S^2\rangle$ have been somewhat overestimated, as seen from Figure 5 of ref 1 and Figure 1 of ref 2, although those of A_2 agree with ours within experimental error.

For comparison, HW theory values of Ψ for a-PαMS are plotted against α_S^3 in Figure 9. They have been calculated from eq 25 with eqs 7−17 and 26 and with $\langle S^2\rangle_0$ for the HW chain given by[4]

$$\langle S^2\rangle_0 = \lambda^{-2} f_S(\lambda L; \lambda^{-1}\kappa_0, \lambda^{-1}\tau_0) \qquad (29)$$

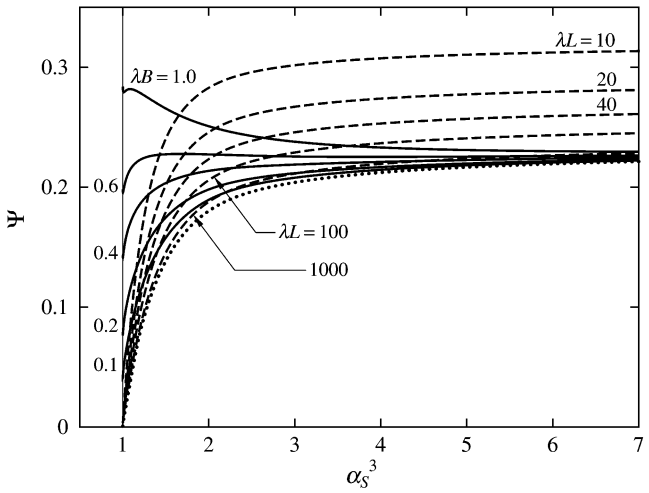

Figure 9. Plots of the theoretical Ψ against α_S^3 for a-PαMS. The solid and dashed curves represent the values at constant λB and λL, respectively. The dotted curve represents the TP theory values.

where the function $f_S(L;\kappa_0,\tau_0)$ of (reduced) L, κ_0, and τ_0 denotes the (reduced) $\langle S^2\rangle_0$ and is given by

$$f_S(L;\kappa_0,\tau_0) = \frac{{\tau_0}^2}{\nu^2} f_{S,KP}(L) + \frac{{\kappa_0}^2}{\nu^2}\left[\frac{L}{3r}\cos\varphi - \frac{1}{r^2}\cos(2\varphi) + \frac{2}{r^3 L}\cos(3\varphi) - \frac{2}{r^4 L^2}\cos(4\varphi) + \frac{2}{r^4 L^2}e^{-2L}\cos(\nu L + 4\varphi)\right] \quad (30)$$

with

$$\nu = ({\kappa_0}^2 + {\tau_0}^2)^{1/2}$$
$$r = (4 + \nu^2)^{1/2}$$
$$\varphi = \cos^{-1}(2/r) \quad (31)$$

In eq 30, the function $f_{S,KP}(L)$ of (reduced) L represents the (reduced) $\langle S^2\rangle_0$ for the Kratky−Porod wormlike chain[4,35] and is given by[4,36]

$$f_{S,KP}(L) = \frac{L}{6} - \frac{1}{4} + \frac{1}{4L} - \frac{1}{8L^2}(1 - e^{-2L}) \quad (32)$$

In the calculation, we have used the above-mentioned values of the HW model parameters. In Figure 9, the solid curves represent the values for the case in which λL (or M) is changed at constant λB, while the dashed curves represent the values for the case in which λB is changed at constant λL (or M). The dotted curve represents the TP theory values as in Figure 8. The left end of each solid curve at $\alpha_S^3 = 1$ corresponds to $\lambda L = 1$. It is seen that the TP theory prediction is obtained as the asymptotic limit of $\lambda L \to \infty$ or $\lambda B \to 0$, and that for finite λB and λL, Ψ always deviates upward from the TP theory prediction. It is also seen that as α_S^3 is decreased, Ψ at constant λB decreases monotonically or after passing through a maximum, and that as α_S^3 is increased from unity, Ψ at constant λL increases more rapidly with larger slope for smaller λL (or M). All these features of Ψ as a function of α_S^3 are in semiquantitative agreement with experiment, as seen from a comparison of Figure 8 with Figure 9.

Finally, we make a comparison of the present results for Ψ for a-PαMS with the previous ones for a-PS[4,7,8] and a-PMMA.[4,9] Figure 10 shows plots of Ψ against α_S^3 for a-PαMS in toluene at 25.0 °C (circles), a-PS in toluene at 15.0 °C (squares), and a-PMMA in acetone at 25.0 °C (triangles), all in the range $\lambda L \gtrsim 1$. The solid, dashed, and dot−dashed curves connect smoothly the data points for a-PαMS, a-PS, and a-PMMA, respectively, and the dotted curve represents the TP theory values as in Figures 8 and 9. The plot for a-PαMS has been reproduced from Figure 8, and those for a-PS and a-PMMA have been reproduced from refs 8 and 9, respectively. The plot for a-PαMS as a whole lies between those for a-PS and a-PMMA. The plot for a-PS exhibits a minimum at $\alpha_S^3 \simeq 1.1$, while those for a-PαMS and a-PMMA do not. This difference may be regarded as arising from the fact that both the a-PαMS and a-PMMA chains are rather stiff and of strong helical nature,[4] as mentioned in the previous paper,[1] while the a-PS chain is rather flexible and of weak helical nature. The plot for a-PMMA decreases monotonically with decreasing α_S^3 and does not exhibit a maximum such as observed for a-PαMS. This is due to the fact that the value 0.22 of λB for a-PMMA in acetone at 25.0 °C is appreciably smaller than its value 0.43 for a-PαMS in toluene at 25.0 °C.

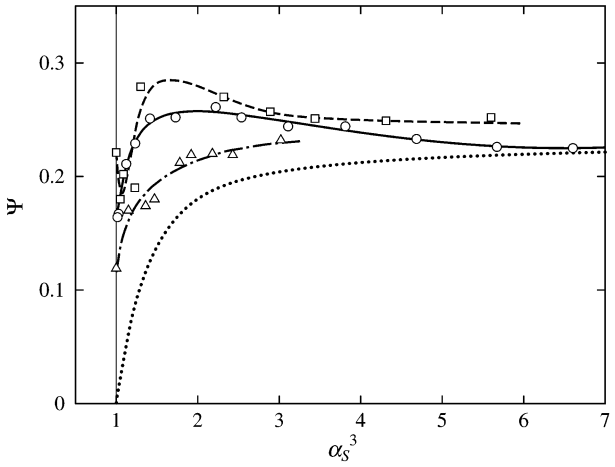

Figure 10. Plots of Ψ against α_S^3: (○) present data for a-PαMS in toluene at 25.0 °C; (□) a-PS in toluene at 15.0 °C;[4,7,8] (△) a-PMMA in acetone at 25.0 °C.[4,9] The solid, dashed, and dot−dashed curves connect smoothly the data points for a-PαMS, a-PS, and a-PMMA, respectively. The dotted curve represents the TP theory values.

Concluding Remarks

We have determined A_2 from light scattering measurements for a-PαMS in the Θ and good solvents over a wide range of M_w, including the oligomer region. The plot of $A_{2,\Theta}$ against M_w in the Θ state, i.e., in cyclohexane at 30.5 °C has been found to exhibit a rather long-tailed negative region for large M_w as well as a sharp increase with decreasing M_w for small M_w, the latter having already been observed for a-PS and a- and i-PMMAs. Such characteristic behavior may be well explained by the theory that takes account of the effects of chain ends and also of three-segment interactions. Then the behavior of A_2 in toluene may be well explained by the HW theory that takes account of the effects of chain stiffness and chain ends in the binary cluster approximation. From the plots of Ψ against α_S^3, it has been reconfirmed that neither the TP nor the QTP theory can explain the behavior of Ψ. The differences in the behavior of Ψ between a-PαMS, a-PS, and a-PMMA

arise from those in chain stiffness, local chain conformation, and reduced excluded-volume strength.

We will proceed to make a study of A_2 near the Θ temperature and of the third virial coefficient in forthcoming papers.

Acknowledgment. This research was supported in part by the 21st century COE program COE for a United Approach to New Materials Science from the Ministry of Education, Culture, Sports, Science, and Technology, Japan.

References and Notes

(1) Osa, M.; Yoshizaki, T.; Yamakawa, H. *Macromolecules* **2000**, *33*, 4828 and succeeding papers.
(2) Osa, M.; Ueno, Y.; Yoshizaki, T.; Yamakawa, H. *Macromolecules* **2001**, *34*, 6402.
(3) Tominaga, Y.; Suda, I.; Osa, M.; Yoshizaki, T.; Yamakawa, H. *Macromolecules* **2002**, *35*, 1381.
(4) Yamakawa, H. *Helical Wormlike Chains in Polymer Solutions*; Springer: Berlin, 1997.
(5) Yamakawa, H. *Modern Theory of Polymer Solutions*; Harper & Row: New York, 1971. Its electronic edition is available on-line at the URL: http://www.molsci.polym.kyoto-u.ac.jp/archives/redbook.pdf.
(6) Yamakawa, H. *Macromolecules* **1992**, *25*, 1912.
(7) Yamakawa, H.; Abe, F.; Einaga, Y. *Macromolecules* **1993**, *26*, 1898.
(8) Einaga, Y.; Abe, F.; Yamakawa, H. *Macromolecules* **1993**, *26*, 6243.
(9) Abe, F.; Einaga, Y.; Yamakawa, H. *Macromolecules* **1994**, *27*, 3262.
(10) Kamijo, M.; Abe, F.; Einaga, Y.; Yamakawa, H. *Macromolecules* **1995**, *28*, 4159.
(11) Cherayil, B. J.; Douglas, J. F.; Freed, K. F. *J. Chem. Phys.* **1985**, *83*, 5293.
(12) Nakamura, Y.; Norisuye, T.; Teramoto, A. *Macromolecules* **1991**, *24*, 4904.
(13) Yamakawa, H.; Yoshizaki, T. *J. Chem. Phys.* **2003**, in press.
(14) Osa, M.; Sumida, M.; Yoshizaki, T.; Yamakawa, H.; Ute, K.; Kitayama, T.; Hatada, K. *Polym. J.* **2000**, *32*, 361.
(15) Suda, I.; Tominaga, Y.; Osa, M.; Yoshizaki, T.; Yamakawa, H. *Macromolecules* **2000**, *33*, 9322.
(16) Deželić, Gj.; Vavra, J. *Croat. Chem. Acta* **1966**, *38*, 35.
(17) Rubingh, D. N.; Yu, H. *Macromolecules* **1976**, *9*, 681.
(18) Berry, G. C. *J. Chem. Phys.* **1966**, *44*, 4550.
(19) Bawn, C. E. H.; Freeman, R. F. J.; Kamalidin, A. R. *Trans. Faraday Soc.* **1950**, *46*, 862.
(20) Einaga, Y.; Abe, F.; Yamakawa, H. *J. Phys. Chem.* **1992**, *96*, 3948.
(21) Yamakawa, H.; Abe, F.; Einaga, Y. *Macromolecules* **1994**, *27*, 5704.
(22) Nakamura, Y.; Inoue, N.; Norisuye, T.; Teramoto, A. *Macromolecules* **1997**, *30*, 631.
(23) Yamakawa, H. *J. Chem. Phys.* **1966**, *45*, 2606.
(24) Yamakawa, H.; Stockmayer, W. H. *J. Chem. Phys.* **1972**, *57*, 2843.
(25) Yamakawa, H.; Shimada, J. *J. Chem. Phys.* **1985**, *83*, 2607.
(26) Shimada, J.; Yamakawa, H. *J. Chem. Phys.* **1986**, *85*, 591.
(27) Domb, C.; Barrett, A. J. *Polymer* **1976**, *17*, 179.
(28) Yamakawa, H.; Abe, F.; Einaga, Y. *Macromolecules* **1994**, *27*, 3272.
(29) Abe, F.; Einaga, Y.; Yamakawa, H. *Macromolecules* **1995**, *28*, 694.
(30) Abe, F.; Einaga, Y.; Yoshizaki, T.; Yamakawa, H. *Macromolecules* **1993**, *26*, 1884.
(31) Tamai, Y.; Konishi, T.; Einaga, Y.; Fujii, M.; Yamakawa, H. *Macromolecules* **1990**, *23*, 4068.
(32) Yamakawa, H.; Yoshizaki, T. *J. Chem. Phys.* **2003**, *118*, 2911.
(33) Yamamoto, A.; Fujii, M.; Tanaka, G.; Yamakawa, H. *Polym. J.* **1971**, *2*, 799.
(34) Kato, T.; Miyaso, K.; Noda, I.; Fujimoto, T.; Nagasawa, M. *Macromolecules* **1970**, *3*, 777.
(35) Kratky, O.; Porod, G. *Recl. Trav. Chim. Pays-Bas* **1949**, *68*, 1106.
(36) Benoit, H.; Doty, P. *J. Phys. Chem.* **1953**, *57*, 958.

MA034481T